Measurement of low-activity uranium contamination by gamma-ray spectrometry for nuclear decommissioning

Nicolas Dufour, Jonathan Dumazert, Eric Barat, Guillaume Bertrand, Frédérick Carrel, Thomas Dautremer, Frédéric Lainé, Adrien Sari

Measurement of Low-Activity Uranium Contamination by Gamma-Ray Spectrometry for Nuclear Decommissioning

N. Dufour*[1], J. Dumazert[1], E. Barat[2], G. H. V. Bertrand[1], F. Carrel[1], T. Dautremer[2], F. Lainé[1], A. Sari[1]

[1]CEA, LIST, Laboratoire Capteurs et Architectures Electroniques, 91191 Gif-sur-Yvette, France.

[2] CEA, LIST, Laboratoire Modélisation et Simulations de Systèmes, 91191 Gif-sur-Yvette, France.

nicolas.dufour3@cea.fr

Abstract

Nuclear decommissioning takes places after dismantling, and consists of studying the possible presence of any residual contamination. To do so, every surface inside the facility must be radiologically characterized, and every contamination removed. In the case of an alpha contamination linked with a low gamma activity, using a High-Purity Germanium detector (HPGe) combined with hypothesis tests on the count statistics can be helpful to assess said contamination. Gamma-ray activity enables to determine the total contamination activity provided both are related, like in the case of an uranium-based contamination. Hypothesis tests determine the statistical power of the measurement, allowing decision making when dealing with countings below the detection limit. A representation of the tests results using Receiver Operating Characteristics (ROC) curves allow the user to select an appropriate time of measurement, true detection and false alarm rates, in accordance to the required specifications. This paper presents the feasibility study of such a method, applied to the detection of a low-activity gamma surface contamination of uranium on concrete, with varying enrichment levels.

I. Introduction

Nuclear decommissioning and dismantling is a process that occurs after a basic nuclear facility is closed [1]. Depending on the past operations conducted in the facility, different contaminations may be expected. Uranium-based contamination, in particular, emits three main signals: alpha particles [2], beta particles [3] and gamma rays [4]. Since all three come from the same decay chain, consequently, determining either activity can lead to the total contamination activity. Alpha spectroscopy and counting is greatly impaired due to rough surfaces leading to different source-detector distances, and the matrix stopping power when the contamination is not strictly a plane surface. Beta counting is sensitive to gamma background signal, coming from either the contamination or the environment. Moreover, at higher uranium enrichments, beta activity is reduced. In fact, the decay chain of uranium 235, when in secular equilibrium, has a low beta and gamma activity relative to the alpha activity, of a factor 10 to 100 depending on the enrichment level. Gamma-ray spectrometry can be used, since gamma rays are weakly affected by variations in source-detector distance.

Using high-resolution gamma-ray detectors, such as the High-Purity Germanium detector (HPGe), we can measure the uranium gamma activity. A high resolution is needed to select narrow regions of interest, associated with gamma peaks of specific uranium radionuclides. Indeed, we can consider three isotopes: uranium 234, 235 and 238, each with specific gamma emissions. Furthermore, in a concrete environment, the signal-to-noise ratio is high, implying high detection limits. This is true when the measured signal originates from a low activity, which is the case in our uranium contamination context, especially with high enrichment levels.

To counter the limitation of standard decision procedures, specific hypothesis tests are used. These give access to a calculation of the statistical power of the measurement, allowing the user to know the confidence interval expressed as true positives or false positives (also called true detections and false alarms). Using simulated and experimental data, we tested the method. The experimental measurements were conducted in a representative basic nuclear facility. We chose as our surface contamination limit for a low activity, close to the background signal:

$$A = 2000\ \text{Bq/m}^2\ (\alpha),\ \Omega = 2\pi\ \text{sr}$$

Where A is the activity and Ω is the solid angle of emission of the source. In this paper, we describe the method and simulations conducted in order to detect low-activity surface gamma contamination using an HPGe spectrometry chain and dedicated hypothesis tests.

II. In-situ gamma spectrometry for nuclear decommissioning and dismantling

The principles of gamma spectrometry have already been well defined in dedicated literature [5]. There are two main detectors used for gamma spectrometry: scintillators and semi-conductors. The difference in performance between these two detectors lies in the underlying physics of signal generation. Scintillation detectors generate a signal with the scintillation photons converted to electrical current using a photodetector such as a photomultiplier or a photodiode, whereas semi-conductors directly collect the charges created by the photon-matter interaction.

Scintillation pulses are short in comparison with semi-conductor ones, meaning scintillators are well suited to handle high-rate counting. They can be produced in large volumes, especially NaI and organic scintillators. On the contrary, semi-conductors have generally a higher resolution than scintillators. Some semi-conductors like CdTe or CdZnTe can be operated at room temperature, while germanium crystals are mostly operated cooled down in order to improve the resolution [6]. These characteristics lead us to choose an HPGe detector for our study, allowing us to define narrower regions of interest, which in result, lowers the minimal detectable activity.

Gamma spectrometry can be used to conduct radiological characterization operations in order to dismantle and/or decommission nuclear facilities. Such operations can be conducted in a laboratory using samples taken from the site, or measurements can be made directly on site [7]. For *in-situ* measurements, both scintillators and semi-conductors are used, predominantly NaI scintillators and HPGe detectors, while for laboratory measurements on samples, high-resolution detectors such as HPGe are preferred [8]. Depending on the expected activity, a calculation of the minimal detectable activity (MDA) must be made prior of the *in-situ* measurements for either NaI or HPGe, either experimentally or using Monte Carlo simulations [9]. Dedicated software have been developed to help the characterization of complex geometries, for example, the In-Situ Object Counting System software [10]. It allows a calibration of the detector without the need of additional sources, enabling gamma spectrometry in complex detection geometries. Measurements conducted with ISOCS showed good agreement with measurements made in laboratory [11]. When dealing with deep contaminations in concrete, the scattering of gamma rays can hinder the precise localisation of the contamination. Methods using collimators can be employed to counter this effect [12], allowing a better mapping of the contamination [13].

The method presented in this paper focuses on the application of a statistical approach to *in-situ* gamma spectrometry measurements, in order to detect low-activity contaminations. Being a post-processing methodology, the statistical approach can be complimentary to other measurements schemes including the use of passive collimators [14] or Compton suppressing systems [15,16], which help reducing the inference from the scattered signal.

III. Source term, concrete background signal and alpha/gamma transfer function

A. Source term: uranium gamma peaks of interest

We use two decay chains to characterize the contamination, and then the mass of uranium present:

Decay chain U-238 :

$$^{238}_{92}\mathrm{U} \rightarrow {}^{234}_{90}\mathrm{Th} + {}^{4}_{2}\alpha\ (4{,}468\ \mathrm{MeV})$$

$$^{234}_{90}\mathrm{Th} \rightarrow {}^{234}_{91}\mathrm{Pa^m} + {}^{0}_{-1}\beta^{-}\ (272\ \mathrm{keV}) + {}^{0}_{0}\overline{\upsilon_e} + \gamma$$
$$\rightarrow {}^{234}_{91}\mathrm{Pa} + {}^{0}_{-1}\beta^{-}\ (272\ \mathrm{keV}) + {}^{0}_{0}\overline{\upsilon_e} + \gamma$$

$$^{234}_{91}\mathrm{Pa^m} \rightarrow {}^{234}_{92}\mathrm{U} + {}^{0}_{-1}\beta^{-}\ (2{,}195\ \mathrm{MeV}) + {}^{0}_{0}\overline{\upsilon_e} + \gamma \ldots$$

Decay chain U-235 :

$$^{235}_{92}\mathrm{U} \rightarrow {}^{231}_{90}\mathrm{Th} + {}^{4}_{2}\alpha\ (4{,}6783\ \mathrm{MeV}) + \gamma$$

$$^{231}_{90}\mathrm{Th} \rightarrow {}^{231}_{90}\mathrm{Pa} + {}^{0}_{-1}\beta^{-}\ (391{,}6\ \mathrm{keV}) + {}^{0}_{0}\overline{\upsilon_e} + \gamma \ldots$$

The major gamma rays studied are extracted from the nuclear database LARA and reported in table I [17].

Table I. Main gamma rays in ^{235}U/^{238}U decay chains

Energy (keV)	Emitter parent isotope	Decay chain	Daughter isotope emission rate per parent isotope decay
49.55(6)	U-238 (γ)	U-238	$6.97(26)\cdot10^{-4}$ (U-238)
113.5(1)	U-238 (γ)	U-238	$1.74(47)\cdot10^{-4}$ (U-238)
63.30(2)	Th-234 (γ)	U-238	$3.75(8)\cdot10^{-2}$ (Th-234)
92.38(1)	Th-234 (γ)	U-238	$2.18(19)\cdot10^{-2}$ (Th-234)
92.80(2)	Th-234 (γ)	U-238	$2.15(19)\cdot10^{-2}$ (Th-234)
766.361(20)	Pa-234m (γ)	U-238	$3.23(4)\cdot10^{-3}$ (Pa-234m)
1001.026(18)	**Pa-234m (γ)**	**U-238**	**$8.47(8)\cdot10^{-3}$ (Pa-234m)**
109.19(7)	U-235 (γ)	U-235	$1.66(13)\cdot10^{-2}$ (U-235)
143.767(3)	**U-235 (γ)**	**U-235**	**$1.094(6)\cdot10^{-1}$ (U-235)**
163.356(3)	**U-235 (γ)**	**U-235**	**$5.08(3)\cdot10^{-2}$ (U-235)**
185.720(4)	**U-235 (γ)**	**U-235**	**$5.70(3)\cdot10^{-1}$ (U-235)**
202.12(1)	U-235 (γ)	U-235	$1.08(2)\cdot10^{-2}$ (U-235)
205.316(4)	**U-235 (γ)**	**U-235**	**$5.02(3)\cdot10^{-2}$ (U-235)**

The methodology to choose which gamma-rays are selected is based on the calculation of the Signal-to-Noise Ratio (SNR):

$$SNR = \frac{N_{signal}}{\sigma_{signal}} = \frac{N_{signal}}{\sqrt{N_{total} + N_{BCKG}}} \quad (1)$$

With N_{signal} the net counting of the full energy peak, σ_{signal} the standard deviation of N_{signal}, N_{total} the total counting of the gamma-ray energy, and N_{BCKG} the counting of the gamma-ray energy corresponding to the background.

We want to maximise the SNR. Based on the variables involved in the SNR formula, we can either increase N_{signal}, decrease N_{BCKG}, or do both. We cannot use the time of measurement to help, since we are looking to minimise it so the total radiological characterization is the lowest possible.

To increase N_{signal}, we can:

Choose a gamma ray with a high emission intensity

Choose a gamma ray with an energy corresponding to the maximum efficiency of the HPGe

To decrease N_{BCKG}, we can:

Choose a gamma-ray far from the maximum background intensity

For example, if we consider the 185 keV gamma ray, it has an emission intensity of $5.7.10^{-1}$, and is located inside the maximum efficiency energy range of the HPGe detector. Both these variables are able to uneven the high background counting rate, creating a contrast. This can be seen in Fig. 6, where the peak clearly emerges from the background base line. For the 1001 keV gamma ray, it is located in an energy range where the background counting rate is at its minimal, creating a visible contrast while having a low emission intensity and being far from the highest detection efficiency energy range of the HPGe. This can be seen in Fig. 7.
We chose to take also into account the 143 keV gamma ray. Its energy is close to the 185 keV, but its emission intensity is five times lower. Little contrast is made (cf. Fig. 6), meaning the SNR is defavorable. The same reasoning was made for the choice of the 163 and the 205 keV gamma rays. We chose to keep these rays to study their impact on the methodology presented here.

We will use the following gamma rays in order to quantify the uranium activity, based on our methodology and the literature:

- 143.767 keV, 163.356 keV, 185.72 keV, 205.316 keV for ^{235}U [18]
- 1001.026 keV for ^{238}U [19]

X rays emitted by the uranium atoms are dismissed in this study, as they do not carry any isotopic information, which consequently provides us no indication on the ^{235}U enrichment level.

B. Background signal: concrete compound environment

The measurement usually needs to be carried out in a closed environment, surrounded by concrete from the walls, ceilings and floors. Henceforth, we have some prior knowledge of the shape, *i.e* normalised spectral distribution, of the background signal. In such an environment, indeed ^{40}K and ^{238}U/^{232}Th decay chains dominate the gamma-ray background activity [20,21].

In order to obtain the first experimental data, related to gamma rays inside a concrete closed environment, a measurement series was conducted inside representative nuclear basic facility premises. Acquired data are shown in Fig. 1. The detector used was an n-type HPGe, which has a relative efficiency of 35%, sold by ORTEC under the reference GMX35P4. The signal was shaped using a symmetrical trapezoidal filter, with a rise time of 2 µs and a plateau time equal to 4 µs. Spectra were acquired on 8192 channels, for an energy range lying between 0 and 3 MeV approximatively. Using a ^{137}Cs source, the energy calibration of the spectrometry chain was performed, prior to the measurements. No correction of the dead time is required, since it is under 1 % for both acquisitions. The acquisition time was taken equal to 3600 s.

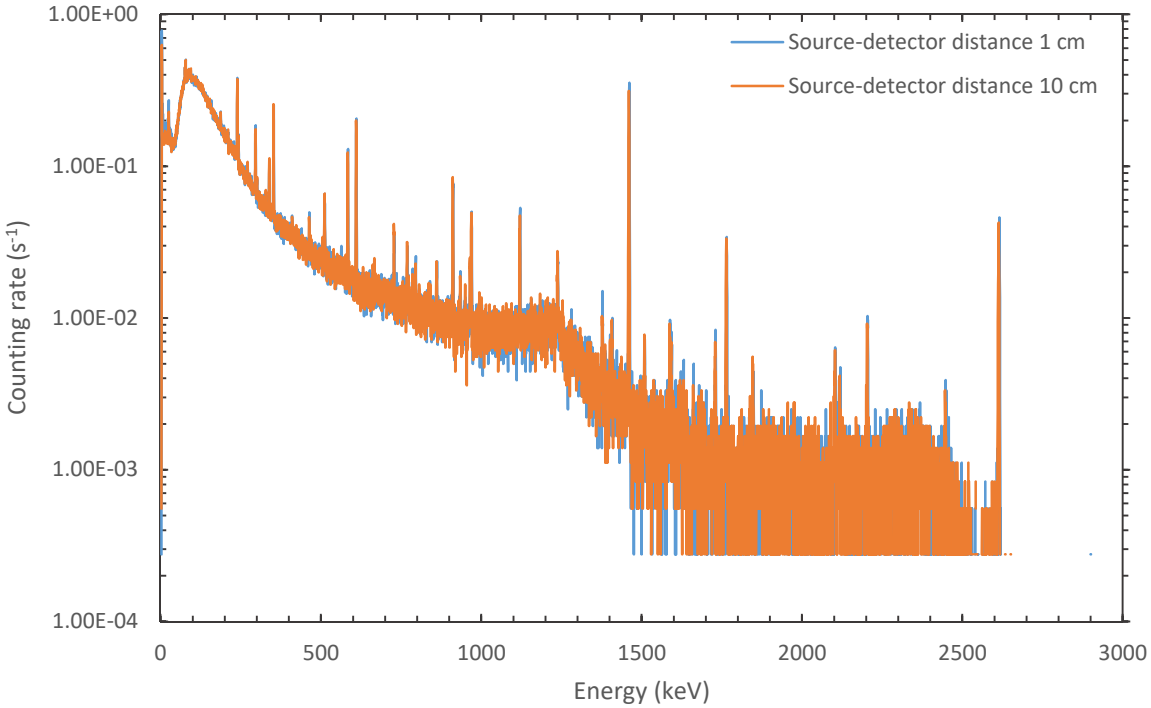

Fig. 1. Counting rate for a concrete closed environment as a function of energy and source-detector distance.

We found no significant difference between a background signal measurement with a distance of one centimetre and a distance of ten centimetres. From now on, we will choose to measure with a distance of one centimetre, in order to maximize the signal of interest. To ensure reliable results, a study of the variability of the background signal, inside the same concrete closed environment, is necessary. To do so, we introduce the following factor of merit, which is a relative deviation:

$$\epsilon[Z] = 100\ \% . \frac{m_{spotA}[Z] - m_{spotB}[Z]}{m_{spotB}[Z]} \quad (2)$$

With $\epsilon[Z]$, the relative deviation associated to a spectral region of interest Z, and m the counting rate associated to a spot. We test any difference in amplitude or shape, using different regions of interest. For amplitude variations, we use the full spectrum, non-normalized. For shape variations, we use regions where a gamma peak of interest is expected or not, normalized. We define those regions as:

- Z_{TOT} = [0 – 3] MeV, region corresponding to the full spectrum

- Z = [140 – 148], [160 - 166], [182 - 188] , [202 – 208], [998 – 1004] keV, regions where a full energy peak of interest from uranium is expected
- W =]1004 – 3000[keV, regions where no full energy peak of interest is expected

The choice of W was made on the assumption that even though there are gamma rays emitted inside this energy range by the uranium decay chain, the emission intensity is lower enough so that their impact is below the statistical variation of the background signal. We will demonstrate that it is the case for our uranium samples measurements presented in part IV. B.

Four measurements were conducted in four different spots, and we compared the acquired data. Table II and III present the factor of merit $\epsilon[Z]$ obtained from one-by-one comparison

Table II. Relative deviations ϵ[Z] between non-normalized responses for different spots of measurements and regions of interest

Spectral region	Spot 1 / Spot 2	Spot 3 / Spot 4
$Z = [0 - 3000\ \text{keV}]$	6.6 %	- 1.1 %
$Z = [140 - 148\ \text{keV}]$	6.2 %	- 2.5 %
$Z = [160 - 166\ \text{keV}]$	6.7 %	- 3.0 %
$Z = [182 - 188\ \text{keV}]$	6.9 %	- 2.2 %
$Z = [202 - 208\ \text{keV}]$	7.7 %	- 5.9 %
$Z = [998 - 1004\ \text{keV}]$	3.2 %	- 9.8 %

Table III. Relative deviations ϵ[Z] between normalized responses for different spots of measurements and regions of interest

Spectral region	Spot 1 / Spot 2	Spot 3 / Spot 4
$Z = [140 - 148\ \text{keV}]$	8.0 %	- 1.5 %
$Z = [160 - 166\ \text{keV}]$	6.7 %	- 2.3 %
$Z = [182 - 188\ \text{keV}]$	7.1 %	- 0.2 %
$Z = [202 - 208\ \text{keV}]$	9.4 %	- 5.8 %
$Z = [998 - 1004\ \text{keV}]$	6.8 %	6.9 %
$W =]1004 - 3000\ \text{keV}]$	7.1 %	0.5 %

We can conclude from tables II and III that the relative deviations are low. The empirical mean of the values is 2.7% and 3.5% in table II and III respectively, while all values are below 10% in absolute value. The means are almost identical, as the extrema of the values, leading us to conclude that the variation in shape and in amplitude are of similar orders.

C. Secular equilibrium and total uranium activity

For any enrichment level, the uranium activity of a contamination A_U can be simplified to the sum of the activities of its three main isotopes, A_{234_U}, A_{235_U} and A_{238_U} :

$$A_{\mathrm{U}} = A_{234_{\mathrm{U}}} + A_{235_{\mathrm{U}}} + A_{238_{\mathrm{U}}} \quad (3)$$

$$A_{235_{\mathrm{U}}}(\gamma) = A_{235_{\mathrm{U}}} . I_{\gamma} \quad (4)$$

Where $A_{235_U}(\gamma)$ is the gamma activity of ^{235}U of a given gamma-ray and I_{γ} is the associated emission intensity. We will consider for this study that the ratio between two enrichment levels is the same for ^{235}U and ^{234}U, meaning that if we determine the enrichment level from ^{235}U and ^{238}U, we can approximate A(^{234}U). We can calculate the gamma activity for the aforementioned emissions, as a function of the enrichment level, for 2000 Bq (α), shown in Fig. 2. Throughout this document, we will use mass concentration (wt%) regarding the enrichment levels.

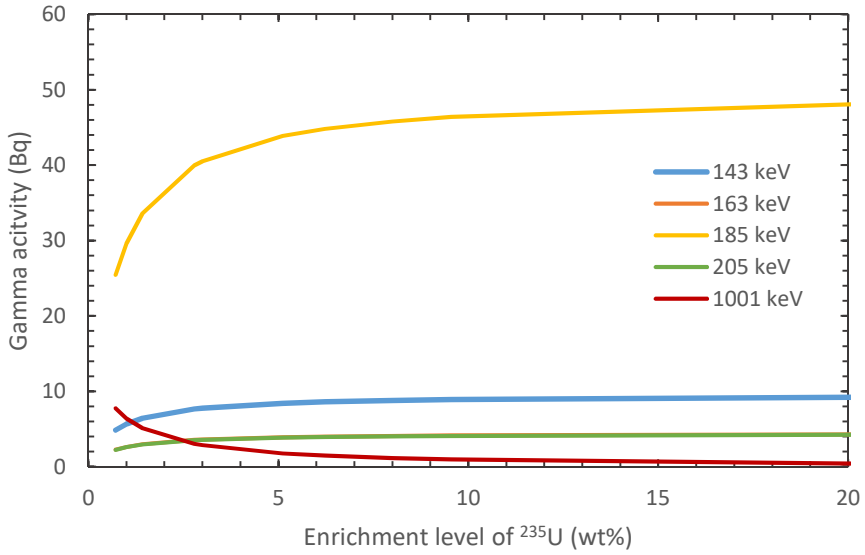

Fig. 2. Gamma activity of the main emission lines of uranium as a function of the enrichment level of ^{235}U, total uranium activity of 2000 Bq (α). Note: 163 keV and 185 keV lines are superimposed.

We have then defined the gamma-ray source term associated to a total activity level. In order to estimate the expected counting rates *in situ*, we now need to introduce a numerical model of the detector and its response to the source term.

IV. Numerical model of the HPGe: modelling and experimental calibration

In order to acquire experimental data, associated to the measurement of uranium samples on a concrete support inside a concrete environment, we launched a series of acquisitions at the Photonic and Irradiation Activation System (*SAPHIR*), located in Saclay at the Atomic Energy Commission [22]. Using the spectrometry chain described in II. B., we placed uranium samples of various enrichment levels in front of a concrete block of one square meter, at a distance of one meter from the detector. No collimator or shielding were used in this study.

A. Numerical model of the detector

We modelled the detector and the series of acquisition using Monte Carlo N-Particles 6 transport code (MCNP6.1) [23]. For our application, we transported the gamma rays, the photons and the electrons created during gamma-matter interaction (mode PE). The modelling was limited to the detector (Germanium crystal and other diode components), the concrete block and the uranium sample. A 3D-visualisation is shown in Fig. 3, made using the visualisation software Vised [24], and table IV introduces the uranium sample used: enrichment level, dimensions, uranium mass and radiological activity.

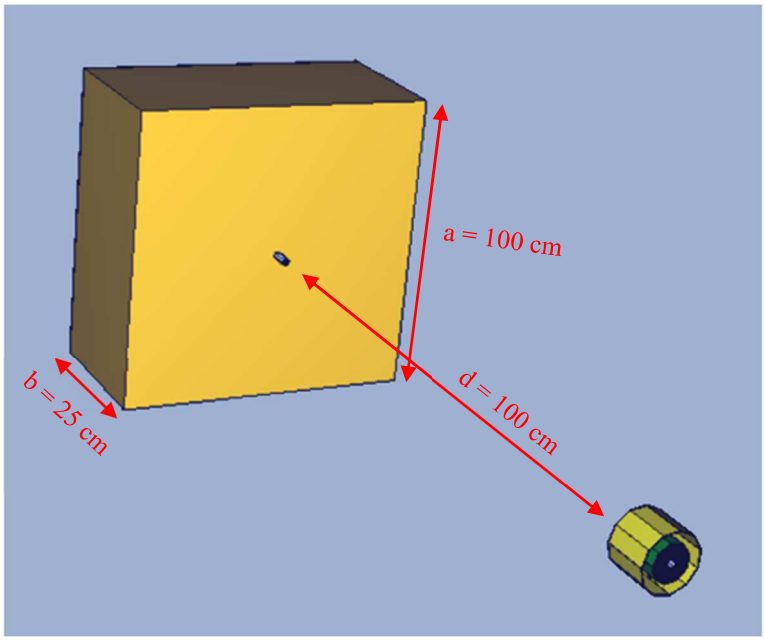

Fig. 3. 3D visualisation of the MCNP6.2 modelling of the experimental setup

Table IV. *Characteristics of the samples measured in SAPHIR and modelled in MCNP6.2*

U-235 enrichment level (wt%)	Diameter (mm) × height (mm)	U-238 mass (mg)	U-238 activity (Bq)	U-235 mass (mg)	U-235 activity (Bq)
0.7112 ± 0.0012	13.1 × 31.5	40764	505496	292	23359
1.416 ± 0.004	13.1 × 31.5	40474	501881	581	46508
2.785 ± 0.013	8.1 × 22.5	10899	135153	312	24980
5.111 ± 0.046	8.1 × 22.5	10639	131920	573	45842
6.222 ± 0.055	8.1 × 22.5	10514	130375	698	55807
9.548 ± 0.121	9.1 × 25.5	14506	179880	1513	122502

To compare the simulations and the experimental acquisitions, we must convert the macroscopic response of MCNP6.2 into an estimated number of events. To do so, we use the activities mentioned in table IV, the gamma emission intensities given by a database and a simulation of the detection efficiency. The chosen database for emission intensities is Nucléide LARA [17], and the spectral response of the detector is given by the tally 8 of MCNP6.1, which gives the number of depositions in an energy bin E_γ, normalized to the number of gamma rays emitted by the source. In order to calculate the number of emitted gamma rays, we use $A_{^{235/238}\mathrm{U}}$ which is the uranium activity considered for an enrichment level, and I_γ, the emission intensity of a specific gamma ray. Such response has been simulated using the energy resolution of the detector. The unit of the tally F8 result, $Y(E_\gamma)$, is then homogenous to a detection efficiency and will be used as such. This simulated detection efficiency also takes into account the energy resolution of the detector, with a Gaussian broadening of the peaks.

We can calculate the simulated number of events as:

$$N_{MCNP}(E_\gamma) = Y(E_\gamma) \cdot A_{^{235/238}\mathrm{U}} \cdot I_\gamma \cdot t \tag{5}$$

With t the time of measurement, taken as 4500 s. The associated uncertainty is calculated using the propagation of uncertainties [25] and gives the following result:

$$\frac{\Delta N_{MCNP}(E_\gamma)}{N_{MCNP}(E_\gamma)} = \sqrt{\left(\frac{\Delta Y(E_\gamma)}{Y(E_\gamma)}\right)^2 + \left(\frac{\Delta A_{^{235/238}\mathrm{U}}}{A_{^{235/238}\mathrm{U}}}\right)^2 + \left(\frac{\Delta I_\gamma}{I_\gamma}\right)^2 + \left(\frac{\Delta t}{t}\right)^2} \tag{6}$$

Fig. 4 and 5 show the simulated data for an enrichment level of 0.7wt% and 9.5wt%, such simulations were also conducted for the other enrichment levels, with the same degree of agreement. Experimental and simulated data are represented with their one standard deviation uncertainties.

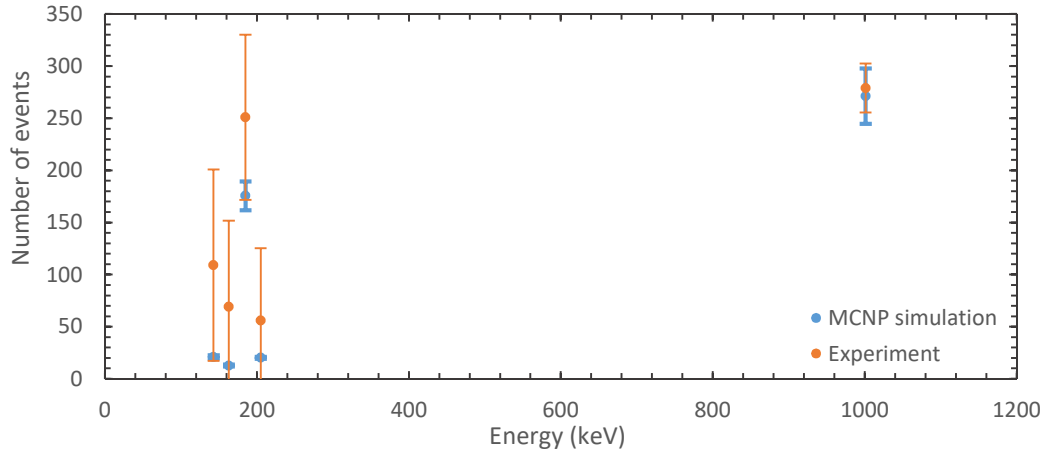

Fig. 4. Number of events expected with an MCNP simulation and experimentally acquired. Enrichment level of 0.7 wt% and time of measurement of 4500 s.

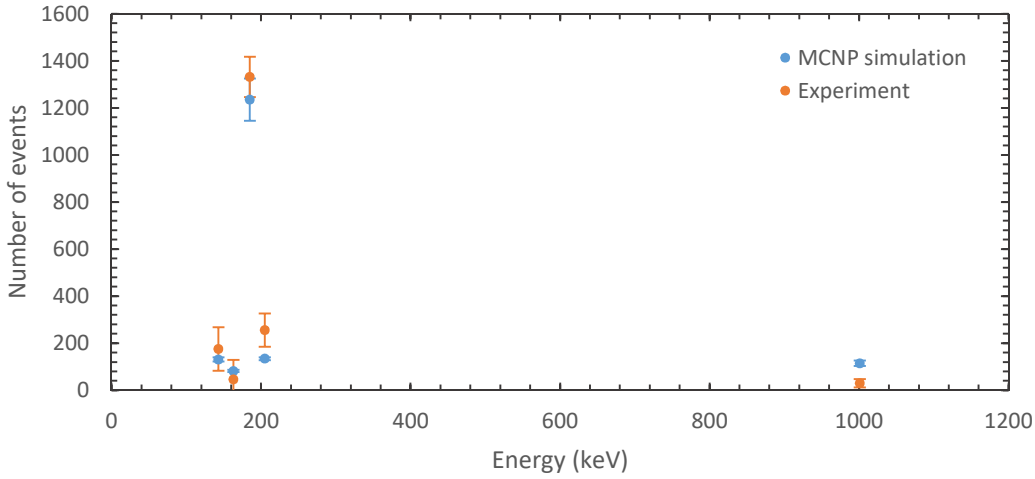

Fig. 5. Number of events expected with an MCNP simulation and experimentally acquired. Enrichment level of 9.5 wt% and time of measurement of 4500 s.

B. Uranium sample measurements in SAPHIR

We acquired a background spectrum and different spectra using varying enrichment level samples. Measurements were performed following a sequential mode: 900 acquisitions of 5 seconds each are summed to form a spectrum of 4500 seconds.

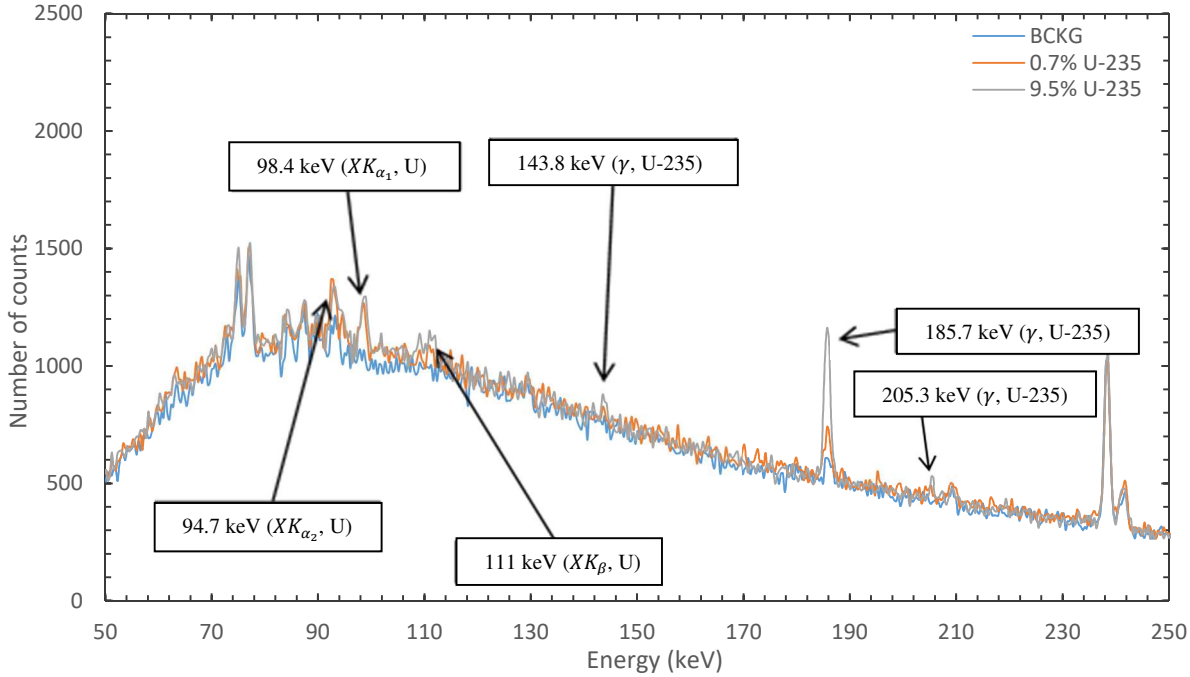

Fig. 6. [50-250] keV cumulated spectra associated to the background signal and the uranium samples of 0.7wt% and 9.5wt% enrichment levels.

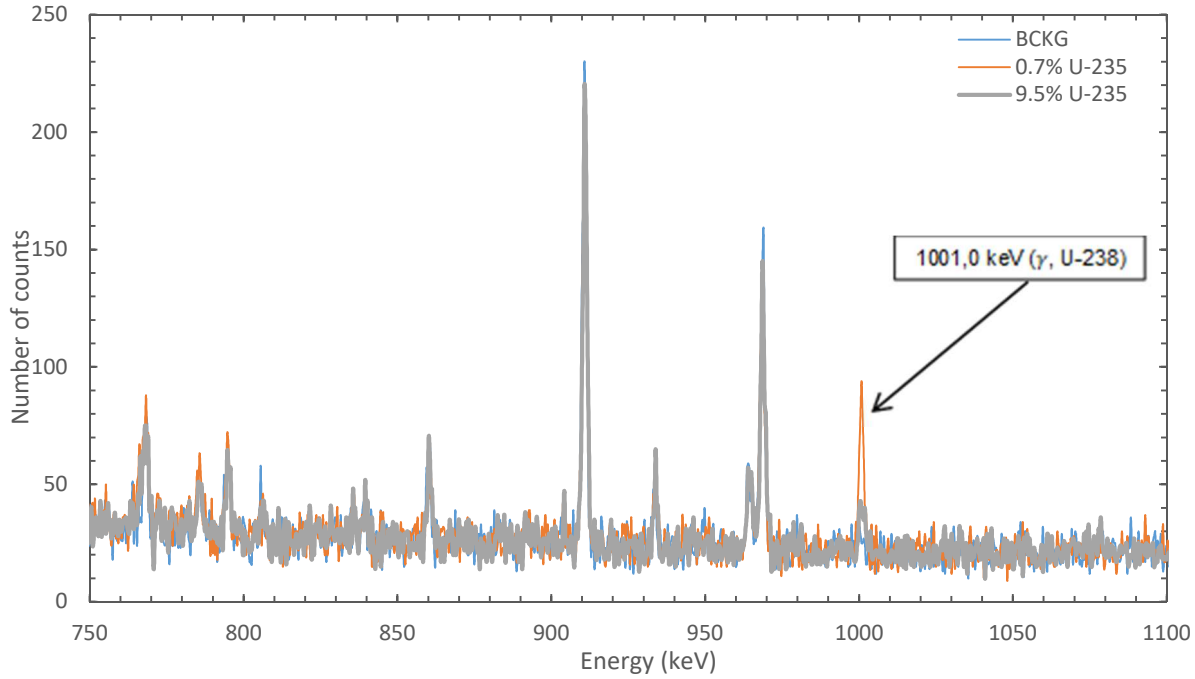

Fig. 7. [750-1100] keV cumulated spectra associated to the background signal and the uranium samples of 0.7wt% and 9.5wt% enrichment levels.

For the ^{238}U, the only gamma peak of interest is 1001.0 keV, emitted when $^{234}U^{*}$, belonging to the ^{238}U decay chain, deexcites into its ground state. The spectral signature of ^{235}U is dominated by the 185.72 keV gamma ray. We mention that the ^{226}Ra, from the ^{238}U decay chain, emits a gamma ray of 186.2 keV energy, which can be seen in the background measurement.

Let $N_{EXP}(E_\gamma)$ be the net experimental response in counts, centred on the energy E_γ. We obtain N_{EXP} by subtracting the background signal spectrum, N_{BCKG}, to the signal spectrum N_{S+BCKG}, and then by integrating the area under the curve, in the associated region of interest. This is shown in equation 6. The response being an histogram with a constant binning, we can simply sum the bins containing 99.7% of the total area (Gaussian approximation). We define the associated one-sigma uncertainty in equation 7.

$$N_{EXP}(E_\gamma) = N_{S+BCKG}(E_\gamma) - N_{BCKG}(E_\gamma) \quad (7)$$

$$\Delta N_{exp}(E_\gamma) = \sqrt{N_{S+BCKG}(E_\gamma) + N_{BCKG}(E_\gamma)} \quad (8)$$

Comparative study and first conclusions

We calculated for all enrichment levels cited in table IV the experimental and simulated responses associated to the five gamma rays of interest for uranium detection: $E_\gamma \in \{143.8; 163.4; 185.7; 205.3; 1001.0\}$ keV. We start by observing that, for a low enrichment level, the simulated responses are much lower than the experimental background signal, for the [140 – 210] keV energy range: as an example, there is over an order of magnitude between the net signal at 185.7 keV and the background signal. This explains the large error bars of one standard deviation observed on Fig. 4.

For all data, we can see that there is an agreement between simulated and experimental data for ^{235}U gamma rays, within two standard deviations, $\pm 2\Delta N_{MCNP}(E_\gamma)$ and $\pm 2\Delta N_{exp}(E_\gamma)$ (Confidence interval of 95% under a Gaussian hypothesis). We also see an agreement for the 238U data for low enrichment levels, but going into higher enrichment levels, experimental and simulated data match within three standard deviations. This result allows us to perform a proof of concept study using this simulation model.

V. Simulated response to the minimal activities to detect

We recall the assumed decommissioning criteria, taken as the minimal surface activity to detect:

A = 2000 Bq (α) / m², Ω = 2π sr

Apart from studying the expected minimal counting rate, we will also study the influence of the presence of another contamination, on an adjacent square meter to the measured one. We test for all gamma rays of interest and for five representative enrichment levels: natural enrichment, 1wt%, 3wt%, 8wt%, 20wt%. We chose a source-detector distance of one centimeter, mentioned before in II. B. Measurements at such a low distance to the surface forces the usage of physical protections for the detector, so as not to damage it while handling and/or moving it to another measurement spot.

Following the conclusions of III. C., we simulate the measurement with a tally F8, which gives us the detection efficiency, and we construct the expected counting rate (s^{-1}), called S, as

$$S(E_\gamma) = Y(E_\gamma) \cdot A_{^{235/238}\mathrm{U}} \cdot I_\gamma \quad (9)$$

depending on the studied gamma ray, whether it is from the ^{238}U decay chain, or the ^{235}U one. The simulated concrete block is 100 × 100 × 25 cm^3. A thickness of 25 centimeters has been chosen for a compromise between the calculation convergence and the accuracy of the concrete background signal [20].

A. *Centred contamination: one centimetre, 2000 Bq (α) / m²*

In this first configuration, the 2000 Bq activity is homogenously spread on the total concrete surface. The symmetry axis of the diode intersects the emitting plan at the center of the concrete surface. We present the geometry diagram on Fig. 8.

In table V, we present the values of $S(185.7\,\mathrm{keV})$ and $S(1001.0\,\mathrm{keV})$, for the considered enrichment levels of ^{235}U. The two responses change, naturally, in the opposite direction when the enrichment increases, since they are the main signatures of the two decay chains.

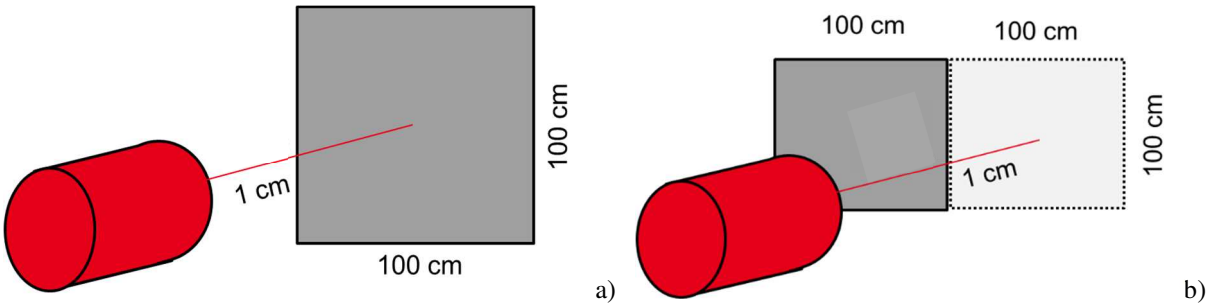

Fig. 8. Simulation geometry diagram for the study of an homogenous surface contamination on one square meter, a) detector centred, b) detector off-centred

Table V. *Evolution of the response S(185.7 keV) and S(1001.0 keV) as a function of the enrichment level. Centred contamination*

Enrichment level	Gamma-ray energy	Detector centred
Natural enrichment	185.7 keV	0.178 ± 0.018 s^{-1}
	1001.0 keV	0.014 ± 0.0014 s^{-1}
1 wt%	185.7 keV	0.20 ± 0.02 s^{-1}
	1001.0 keV	0.011 ± 0.0010 s^{-1}
3 wt%	185.7 keV	0.28 ± 0.02 s^{-1}
	1001.0 keV	0.005 ± 0.0004 s^{-1}
8 wt%	185.7 keV	0.32 ± 0.04 s^{-1}
	1001.0 keV	0.002 ± 0.0002 s^{-1}
20 wt%	185.7 keV	0.34 ± 0.04 s^{-1}
	1001.0 keV	$7.8 \cdot 10^{-4} \pm 8.10^{-5}$ s^{-1}

B. Adjacent contamination: one centimetre, 2000 Bq (α) / m²

In this configuration, we study the impact of the presence of an adjacent contamination. In this case, the contamination is adjacent to the original contamination surface, see Figure 8. b. The goal is to quantify the impact on the measurement of an adjacent surface; in other words, the spatial resolution of the detection method.

Table V and VI present the values of $S(185.7\,keV)$ and $S(1001.0\,keV)$ respectively, for the considered enrichment levels of ^{235}U. Comparing the data in tables V and VI, we observe that the decentring of the detector from the contamination leads to an interference of about 7 ± 1 % of the measured contamination. This result confirms that the influence of an activity-equivalent adjacent contamination is limited and allow us not to use a collimator. However, in the case of a high adjacent contamination or close storage of nuclear waste, a collimator may be needed. The influence of such contaminations is an outlook for future work.

Table VI. *Evolution of the response S(185.7keV) as a function of the enrichment level. Off-centred detector*

Enrichment level	Gamma-ray energy	Off-centred detector
Natural enrichment	185.7 keV	0.0128 ± 0.0012 s^{-1}
	1001.0 keV	$1.0 \cdot 10\text{-}3 \pm 1 \cdot 10^{-4}$ s^{-1}
1 wt%	185.7 keV	0.0147 ± 0.0014 s^{-1}
	1001.0 keV	$8.2 \cdot 10^{-4} \pm 8 \cdot 10^{-5}$ s^{-1}
3 wt%	185.7 keV	0.020 ± 0.002 s^{-1}
	1001.0 keV	$3.8 \cdot 10^{-4} \pm 4 \cdot 10^{-5}$ s^{-1}
8 wt%	185.7 keV	0.022 ± 0.002 s^{-1}
	1001.0 keV	$1.5 \cdot 10^{-4} \pm 1.4 \cdot 10^{-5}$ s^{-1}
20 wt%	185.7 keV	0.024 ± 0.002 s^{-1}
	1001.0 keV	$5.4 \cdot 10^{-5} \pm 6 \cdot 10^{-6}$ s^{-1}

We have defined the source term of a surface uranium contamination, and the background associated to a measurement conducted in a concrete facility. We can now generate representative spectra in order to evaluate the performances of different hypothesis tests, without having to acquire a large number of measurements.

VI. Representative spectra and hypothesis tests

This section is dedicated to the basic description of hypothesis tests [26] used to detect the gamma ray signature of ^{235}U and ^{238}U inside a concrete compound environment. The hypothesis test aim is to decide whether, for a given observation time:

- The detector response is due only to the background signal (Null hypothesis, noted H_0)
- The response reveals the presence of an additional ^{235}U or ^{238}U signal (Alternate hypothesis, noted H_1)

The conditions to accept H_1 govern, in a given measurement time, the best compromise between False Alarm Rate (FAR) and True Detection Rate (TDR). Given that the measurement time is a parameter, we start by describing the principle of a representative spectrum generator, with varying measurement time. We then introduce the three hypothesis tests, which performances have been studied via simulations.

A. Representative spectrum generation

In order to estimate the performances of a given hypothesis test as applied to the reconstitution of a measurement of time t, we need to construct, at least, two spectra representing respectively the background signal and the addition of the background signal with the uranium signal.

We use, as a background signal reference, the spectral response between [0 – 3] MeV acquired in a representative nuclear basic facility, shown in II. B. A background signal measurement will be obtained from a random draw following a Poisson law [26], where the density of probability is identified to the measured background signal spectrum. A signal measurement will be a random draw following a Poisson law, where the density of probability is identified to the sum of the background signal spectrum and the simulated response of the detector, shown in IV. A. To better simulate the spectra, we will use a Gaussian Energy Broadening (GEB) card on MCNP. The input parameters are $a = 0.0007$ MeV and $b = 0.0011\ \mathrm{MeV}^{\frac{1}{2}}$ for a simulated Full Width at Half Maximum $LTMH = f\left(\sqrt{E_\gamma}\right) = a + b\sqrt{E_\gamma}$ [5].

In order to simulate different measurement times, we created a spectrum generator, where the reference counting rates are multiplied with an input time, and the final value is a random draw of a Poisson law where the parameter is the product described before. We generate N spectra for background signal only and N spectra for background signal plus uranium signal, on which the tests will be based. We used $N = 10000$, giving 20000 spectra in total.

B. Hypothesis tests

The fact that we can use physics models to simulate the gamma source term associated to a uranium contamination (II. A. and C.), and that we obtain multichannels spectra from acquisitions, allow an *a priori* modelling of the H_1 hypothesis, and so the usage of Bayesians tests [27]. Such a usage, however, is left as an outlook of this paper, to focus on frequentist tests. Now, we will present some characteristics associated to hypothesis tests before introducing the ones used in this study. Other usage of hypothesis tests are described in the literature [28].

A hypothesis test is said absolute when it is sensitive to any variation of counting rate on the associated regions of interest. Such tests are vulnerable to any variations in amplitude of the background signal. Relative tests, on the contrary, are only affected by a difference in shape of the regions of interest, making them suited in cases of a variation in background signal intensity. We also need to consider the laterality of the hypothesis tests. The conformity of the data to the null hypothesis is given by the p-value. P-values are calculated and compared to a rejection threshold, called the alpha level (α). In a bilateral test, the p-value is rejected when its modulus is superior to α. In a unilateral test, the p-value is rejected if the p-value is superior to α. It is then possible to discriminate a significant increase in the regions of interest from a significant decrease, providing the latter has a physical interpretation.

Three hypothesis tests are presented and their principles explained. We used the Kolmogorov-Smirnov (KS) test [29], a test based on the Cumulative function of a Negative Binomial law (CNB) [30] and a test based on the Cumulative function of a Beta Binomial law (CBB) [31].

Kolmogorov-Smirnov test (KS)

The KS test is the classic relative test in literature, to detect a change in statistical distribution (shape of the spectrum). This test enables to determine whether two statistical samples, in this case the radiological background and a signal measurement, are identically distributed. The counting data, or number of counts, associated to the reference

background spectrum, noted $m_{ref}[E_\gamma]$, and to the measured signal, noted $m_{test}[E_\gamma]$, are classified in a histogram with regular energy bins $E_\gamma \in [0-3]$MeV. We calculate the empirical normalised cumulative functions $c_{ref}[E_\gamma]$ for the reference background spectrum and $c_{test}[E_\gamma]$ for the measured signal of the two data sets:

$$\forall\, E_\gamma \in [0; 3\ \text{MeV}],\ c_{ref}[E_\gamma] = \frac{\sum_{j=0}^{E_\gamma} m_{ref}[j]}{\sum_{j=0}^{3\ \text{MeV}} m_{ref}[j]} \tag{10}$$

$$\forall\, E_\gamma \in [0; 3\ \text{MeV}],\ c_{test}[E_\gamma] = \frac{\sum_{j=0}^{E_\gamma} m_{test}[j]}{\sum_{j=0}^{3\ \text{MeV}} m_{test}[j]} \tag{11}$$

The p-value is given by:

$$p = \max_{0 \le E_\gamma \le 3\ \text{MeV}} \left| c_{test}[E_\gamma] - c_{ref}[E_\gamma] \right| \tag{12}$$

For a fixed α level, the KS hypothesis test reads:
If p > α, the H_0 hypothesis is rejected and a contamination is detected.
Else, H_0 is accepted.

The KS test is bilateral, meaning it is sensitive to any variation to the spectrum shape. We can expect that the compromise between the True Detection Rate (TDR) and the False Alarm Rate (FAR) is inferior to the one a unilateral test can give. This is why we now introduce a unilateral hypothesis test designed to discriminate any increase in the regions of interest.

Test on the Cumulative function of a Negative Binomial law (CNB)

We introduce an absolute and unilateral test, able to differentiate the acquisition times between the reference period (T_{ref}) and the test period (T_{test}). This test is simple in the sense that it only requires a total counting in both the regions of interest of ^{235}U and the region of interest of ^{238}U:

$$Z = [140-148] \bigcup [160-166] \bigcup [182-188] \bigcup [202-208] \bigcup [998-1004]\ \text{keV} \tag{13}$$

The cumulative function is built under the H_0 hypothesis of an identical counting intensity between the two acquisitions. Let $m_{ref}[Z]$ be the associated counting of the reference background signal and $\rho[Z]$ the associated counting rate. The counting $m_{ref}[Z]$ is supposed to follow a Poisson law under the H_0 hypothesis, while its parameter $\rho[Z]$ is supposed to follow a gamma law of parameters $(a\,;b)$. The parameters $(a\,;b)$ are set to represent the absence of any inference on the counting intensity, with values $a = 0.5$ and $b = 0$. [32]

Henceforth, the *a posteriori* law of $\rho[Z]$ knowing $m_{ref}[Z]$ is a gamma law of parameters $(a + m_{ref}[Z]\,; b + T_{ref})$, and the posterior predictive law of $m_{test}[Z]$ knowing $m_{ref}[Z]$ is a negative binomial law of parameters $\left(\frac{T_{test}}{b+T_{ref}+T_{test}}\,; r = a + m_{ref}\right)$. The cumulative function $C[Z]$, associated to this negative binomial law, is given by:

$$C[Z] = 1 - I_p(m_{test}[Z], r) \tag{14}$$

Where I_p is the regularized incomplete beta function of parameters $m_{test}[Z]$ and r. The p-value is then defined as:

$$p = 1 - C[Z] \tag{15}$$

For a fixed α level, the CNB hypothesis test is:
If p > α, the H_0 hypothesis is rejected and a contamination is detected.
Else, H_0 is accepted.

The CNB test is by construction sensitive to any variation in background signal intensity. Now we showed in II. B. that the background intensity can vary from a spot to another, which lead us to introduce a more sophisticated test with respect to background signal variation.

Test on the Cumulative function of a Beta Binomial law (CBB)

Finally, we introduce a relative and unilateral test, relying on a measurement during a time T_{ref} and a signal measurement during a time T_{test}. The test uses the same regions of interest Z described for the CNB test, but also another region of interest, where no signal is expected, named control region. We define such region as:

$$W = \,]1004 - 3000]\ \text{keV} \tag{16}$$

We excluded the interval $[0 - 140[$ keV because of X-ray and low-energy gamma signals, especially the ones corresponding to uranium.

Using the same notations as before, we introduce $m_{ref}[W]$, the counting in the control region of the background signal, and $m_{test}[W]$, the counting in the control region of the measured signal. The CBB test relies on the introduction of a random variable ρ, distributed as a beta law of parameters $(a\,;b)$. We choose $a = 0.5$ and $b = 0.5$, corresponding to the absence of any prior knowledge of ρ [33]. The counting $m_{ref}[Z]$, during a measurement time T_{ref} on the region of interest Z is supposed to follow a binomial law of parameters $\left(m_{ref}[Z] + m_{ref}[W]\,;\rho\right)$. The *a posteriori* law of ρ, knowing $m_{ref}[Z]$ and $m_{ref}[W]$, is then a beta law of parameters $\left(a + m_{ref}[Z]\,;b + m_{ref}[W]\right)$.

Under the H_0 hypothesis, the $m_{test}[Z]$ counting associated to the tested spectrum is distributed following a binomial law of parameter ρ. The predictive posterior law of $m_{test}[Z]$ knowing $m_{ref}[Z]$, $m_{ref}[W]$ and $m_{test}[W]$, is a beta binomial law with a number of draws $k_{test} = m_{test}[Z] + m_{test}[W]$ and parameters $\left(a + m_{ref}[Z]\,;b + m_{ref}[W]\right)$. Finally, the cumulative function associated to this law is expressed as:

$$C[Z,W] = \frac{\mathrm{B}\left(a + m_{ref}[Z] + m_{test}[Z] + 1, b + m_{ref}[W] + m_{test}[W] - 1\right) \cdot F_{k_2}\left(\vec{a},\vec{b},m_{ref}[Z]\right)}{\mathrm{B}\left(a + m_{ref}[Z], b + m_{ref}[W]\right) \cdot \mathrm{B}(m_{test}[W], m_{test}[Z] + 2) \cdot (m_{test}[Z] + m_{test}[W] + 1)} \tag{17}$$

Where B is the beta function and $F_{k_2}\left(\vec{a},\vec{b},m_{ref}[Z]\right)$ is the generalised hypergeometric function ${}_3F_2$.

For a fixed α level, the CBB hypothesis test reads:
If $C[Z,W] < \alpha$, the H_0 hypothesis is rejected and a contamination is detected.
Else, H_0 is accepted.

A study of the control region]1004-3000] keV was made in order to determine if there is a difference in measured background signal with and without a sample, and if this difference is statistically significant. To do so, we sum the spectrum in this area and compare it with the spectra with samples. The results are displayed in figure 9 below:

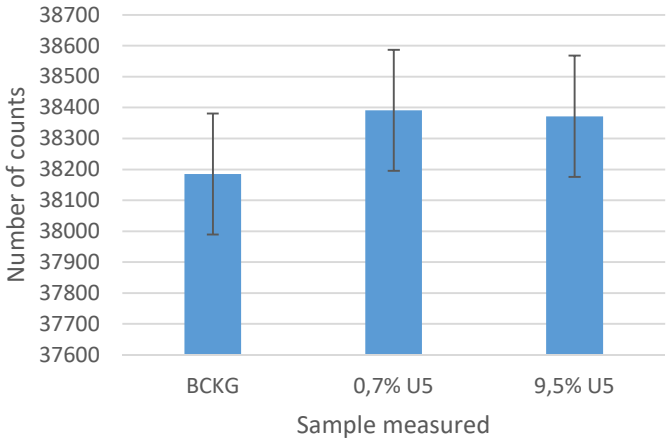

Fig. 9.]1004-3000] keV summed spectra associated to the background signal and the uranium samples of 0.7wt% and 9.5wt% enrichment levels. The uncertainty plotted is one standard deviation.

We can see that all three measurements are under one standard deviation of the background-only measurement. We can conclude that the variation inside the control region is contained under the statistical variation of the background, thus it will have a minor impact on the CBB test.

VII. Receiver Operating Characteristic curves and integration time

The study of the statistical power of the tests presented in V. B. will be conducted, based on the generated representative spectra described in paragraph V using Receiver Operating Characteristic (ROC) curves. Such curves characterize the power of the tests described earlier. The generated spectra allow us to conduct the study without having to acquire multiple spectra on site.

A. ROC curves

Definition of the ROC curve

A ROC curve is the performance graph of a complete detector chain, as a plot of the TDR as a function of the FAR. An ideal detector would present a ROC curve passing through the following points: (0;0) - (0;1) - (1;1), while a random response detector would show a plot consisting of a line crossing (0;0) and (1;1). Hence, in the absence of a preset condition on an acceptable TDR or TDV, hypothesis tests power are evaluated on their ROC curves approaching (0;1) [34].

ROC curves are constructed using a Monte Carlo method. We proceed to sample N random draws in the background signal measurements, and the same number N in the constructed signal spectra from the representative spectra generator described in V. A. The binary result of a test, 1 for a detection and 0 for a non-detection, depend on the chosen alpha level. Therefore, the possible alpha level between 0 and 1 are given with a step of 10^{-6}. For each value, we calculate the number of true positives in the presence of a contamination, corresponding to true detections N_{TD}, and the number of false positives in the absence of a contamination, corresponding to false alarms N_{FA}. We finally calculate, for each alpha level and each hypothesis test, the couple $\left(TDR = \frac{N_{TD}}{N}; FAR = \frac{N_{FA}}{N}\right)$, to which we associate its repeatability one standard-deviation uncertainty:

$$\sigma(TDR) = \sqrt{\frac{1}{N} \cdot TDR \cdot (1 - TDR)}\,; \sigma(FAR) = \sqrt{\frac{1}{N} \cdot FAR \cdot (1 - FAR)} \tag{18}$$

The Monte Carlo method is carried out using MATLAB [35]. The number of iterations is $N = 10000$, so that $\sigma(TDR)$ and $\sigma(FAR)$ do not exceed 0.5 %.

Simulated configurations and Monte Carlo method setup

ROC curves can be traced for different enrichment levels, different backgrounds signals, different measurement times and different hypothesis tests. Moreover, we chose to study the impact of a variation in background amplitude, but not in shape, on the detection performance. To do so, we multiplied to background signal spectra by a factor between 1.01 and 1.1, corresponding to the average 1 % and 10 % maximum orders of variation found in II. B. We are indeed looking to find the most effective test in the case of background signal stability, but also the most resilient when background signal does change in amplitude.

The selected configurations of the variables we have described above are the following:

- Source-detector distance of 1 cm ;
- Enrichment levels: natural enrichment, 1 wt%, 3 wt%, 8 wt%, 20 wt% ;
- Normal background signal, background × 1.01, background × 1.1 ;
- Measurement time $t \in \{100; 200; 300; 500; 1000; 3000\}\ s$;
- Hypothesis tests: KS, CNB, CBB.

This description leads to the generation of 270 ROC curves, from which we can determine tendencies with their associated confidence intervals. We will only display the ROC curves for the modified background signal, with the 1 wt%, 3 wt%, 20 wt% enrichment levels and with simulated measurement times of $\{300; 3000\}$ s. The ROC of the three hypothesis tests are superimposed on every curve.

Results

Figures 10 to 15 show the obtained results from the study aforementioned.

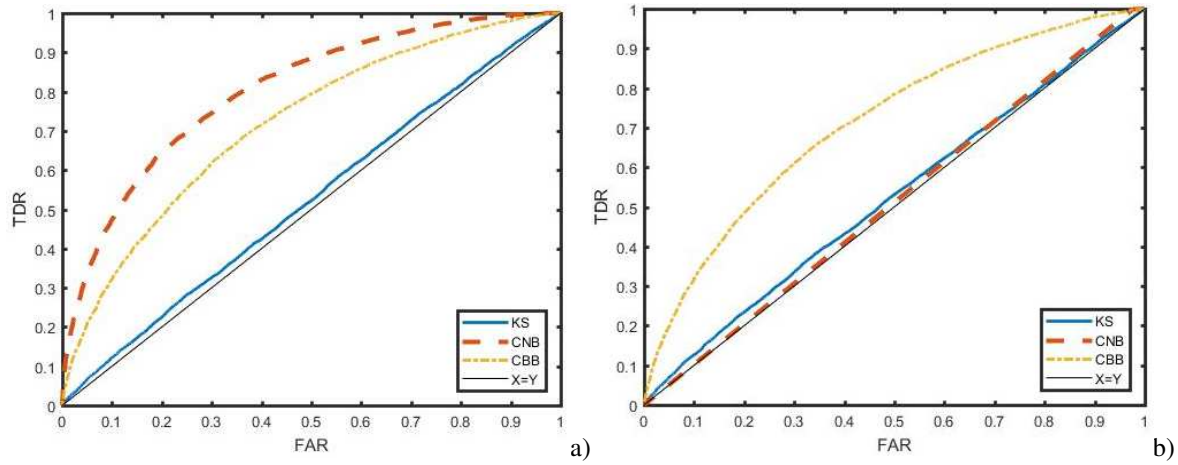

Fig. 10. ROC curve for an enrichment level of 1wt%, $t = 300$ s, with a background multiplied by a) 1.01, b) 1.1

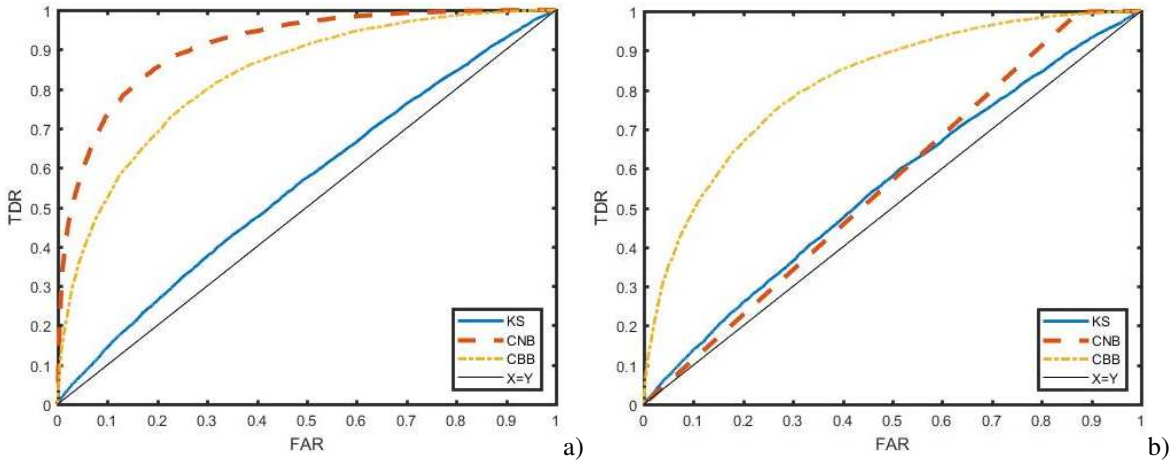

Fig. 11. ROC curve for an enrichment level of 3wt%, $t = 300$ s, with a background multiplied by a) 1.01, b) 1.1

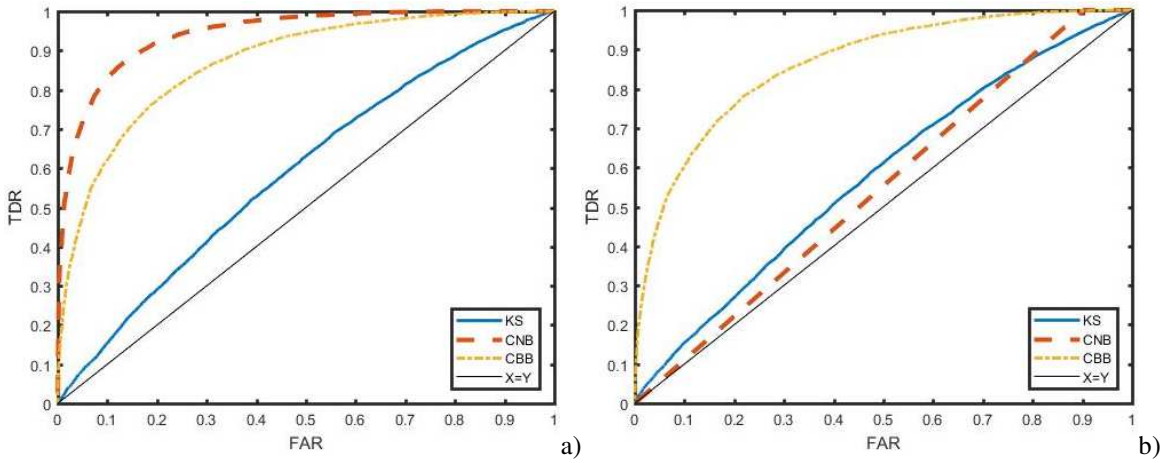

Fig. 12. ROC curve for an enrichment level of 20wt%, $t = 300$ s, with a background multiplied by a) 1.01, b) 1.1

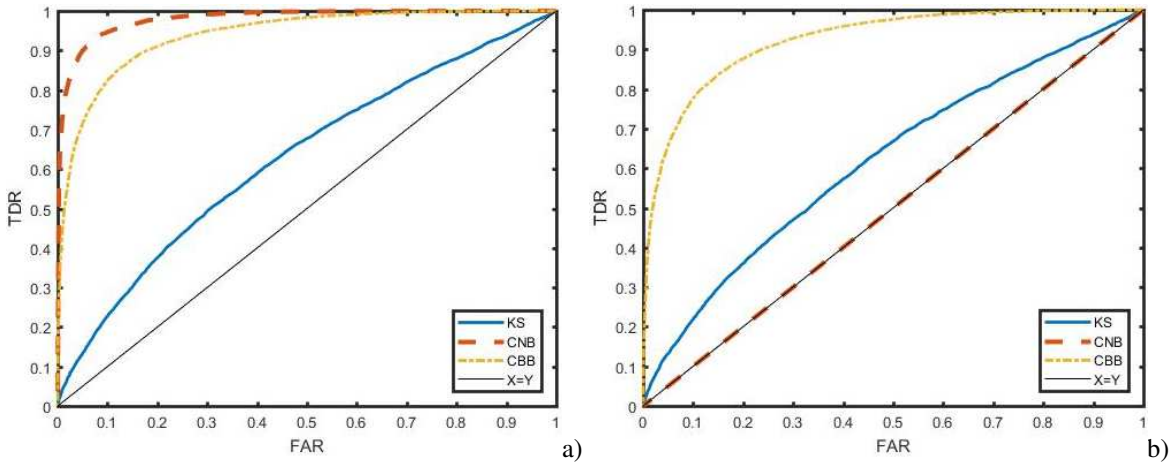

Fig. 13. ROC curve for an enrichment level of 1wt%, $t = 3000$ s, with a background multiplied by a) 1.01, b) 1.1

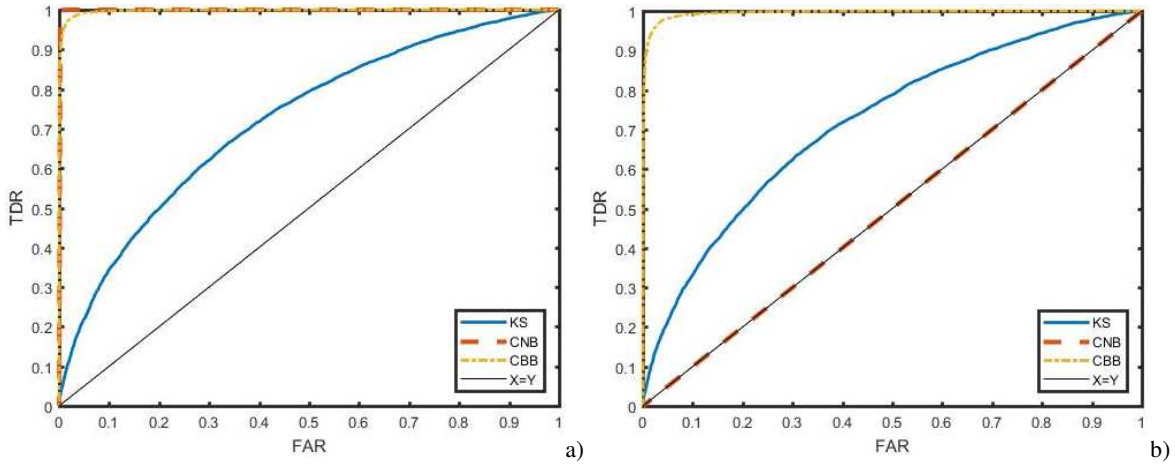

Fig. 14. ROC curve for an enrichment level of 3wt%, $t = 3000$ s, with a background multiplied by a) 1.01, b) 1.1

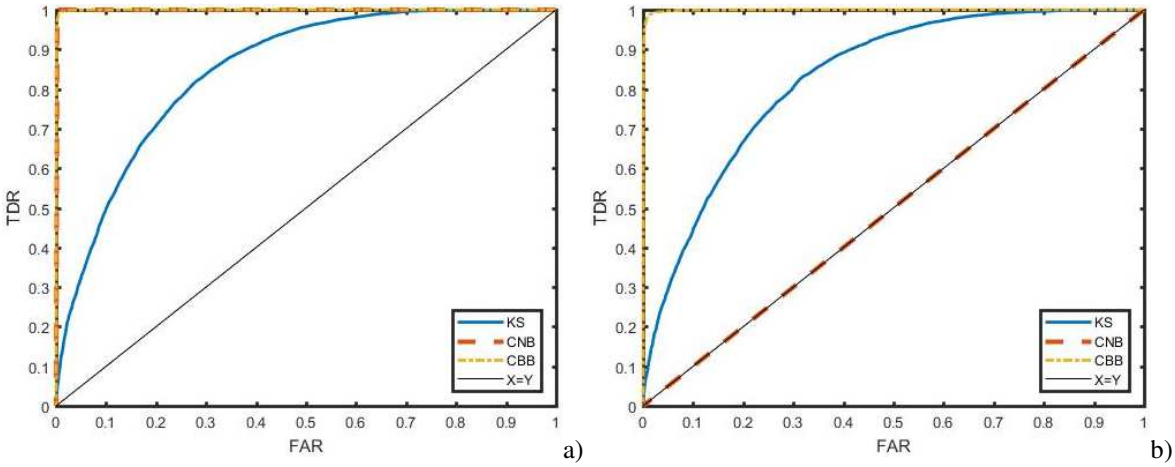

Fig. 15. ROC curve for an enrichment level of 20wt%, $t = 3000$ s, with a background multiplied by a) 1.01, b) 1.1

B. Interpretation of the results

The ROC curves presented above enable to describe explicit trends, which are in adequacy of the description of the hypothesis tests in V. B. According to figures 10 to 15, and also on ROC curves not shown in this paper, we conclude the following:

1) The ROC curves, for each hypothesis test, are more right-angled to the (0;1) point when the enrichment level is high. For example, the comparison of Fig. 10 a) (1wt%) and Fig. 12 a) (20 wt%) show an increase of the TDR – FAR rate, with the CNB test for the closest point to (0;1), (0.23;0.73) and (0.15;0.87) respectively. We explain this phenomenon with the bigger discriminability of the 185.7 keV gamma ray from the ^{235}U decay chain, for higher enrichment levels, shown in Fig. 6.
2) The ROC curves, for each hypothesis test, are more right-angled to the (0;1) point when the simulated measurement time is long. For example, the comparison of Fig. 10 a) ($t = 300$ s) and Fig. 13 a) ($t = 3000$ s) show an increasing of the TDR – FAR rate, with the CBB test for the closest point to (0;1), (0.28;0.65) and (0.07;0.83) respectively. The variance reduction associated to a longer time of measurement explains this result.
3) For a stationary background signal, the CNB test yields better results, being the only absolute and unilateral test. In addition, when the background signal varies slightly (1%), we do not note any variation in performances over the different tests. But when the background varies more significantly (10%), the CNB test performances collapse, which is shown in figures 10 to 15 b). The ROC curve is overlapped with the diagonal (0;0) – (1;1). This is explained with the construction of the CNB test: Absolute test only remain operational under the hypothesis that the background signal is identical between the reference period and the test period. On the other hand, the KS and CBB test performances are not significantly affected by this variation (deviation of 5 %).

As a partial conclusion, the KS test does not ever provide the highest performance in our study, being a bilateral test. Considering all parameters, the relative and unilateral test CBB gives the best compromise between sensibility to the signal and sensibility to the background variations. The ROC curves obtained are close to a perfect ROC curve (5 % close on the TDR – FAR rate) with high enrichment levels (Fig. 14 and 15 a)), considering a measurement time of 3000 s. Yet, when dealing with low enrichment levels, the CBB test performances drop as compared to the ones of the CNB test. Under the assumption that the reference background is truly representative of the measured spectrum, the CNB test can be preferred, else, when dealing with any background signal variation, we suggest using the CBB test.

C. Evolution of the True Detection Rate as a function of the acquisition time

In order to optimise the acquisition time and reduce the decommissioning costs, we studied the variation of the TDR as a function of time with a fixed FAR of 0.5. This represents a risk of 50 % of considering a non-contaminated surface of one square meter as radioactive waste. Using the results obtained for the ROC curves, we constructed different graphs of TDR as a function of time. For visualisation purposes, we will only display some of the results.

Figures 16 and 17 show the results of the study (TDR as a function of the measurement time) for an enrichment level of 1 wt%, with different background signals (reference, and multiplied by 1.1). Figure 18 show the same graph but with an enrichment level of 20 wt% and a background multiplied by 1.1.

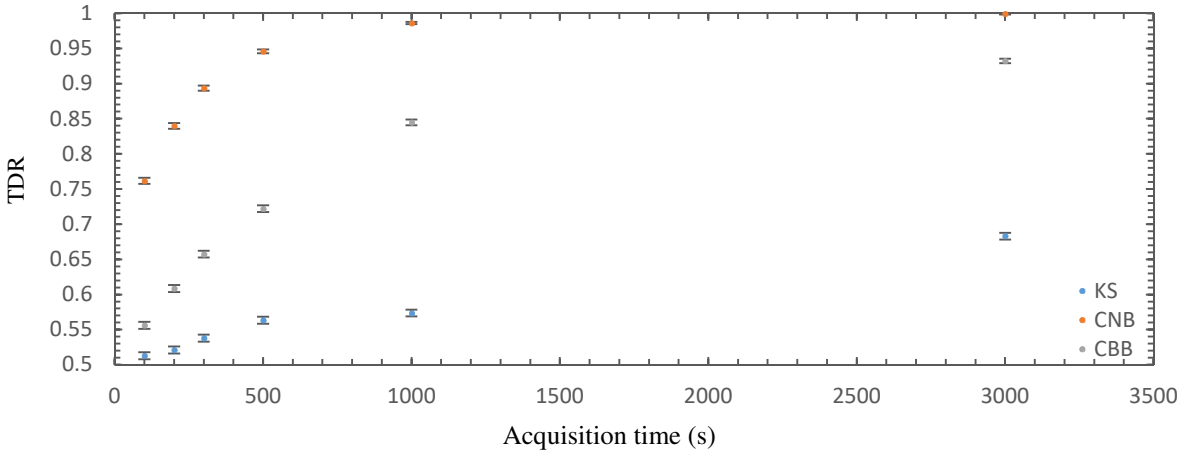

Fig. 16. TDR as a function of the acquisition time, for a FAR of 0.5, enrichment level of 1 wt%, and a reference background

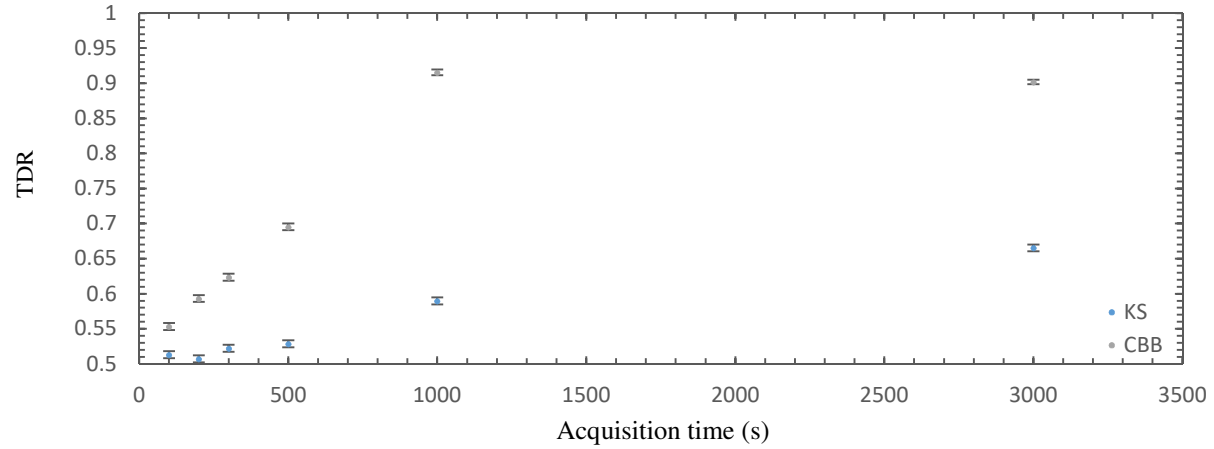

Fig. 17. TDR as a function of the acquisition time, for a FAR of 0.5, enrichment level of 1 wt%, and a background multiplied by 1.1

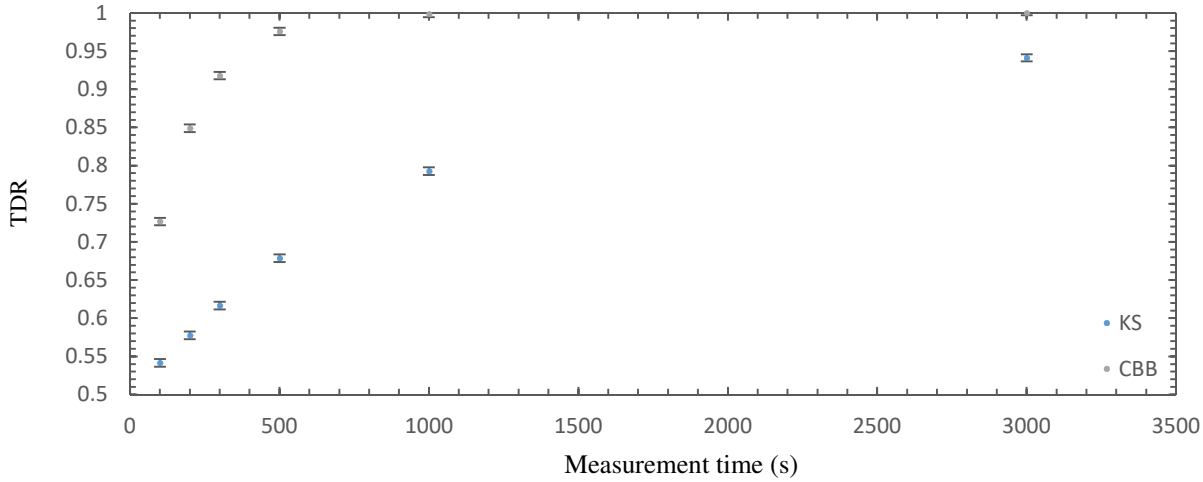

Fig. 18. TDR as a function of the acquisition time, for a FAR of 0.5, enrichment level of 20 wt%, and a background multiplied by 1.1

We make the following observations, based on figures 16 to 18:

1) For an integration time $t = 500$ s and whether the background is multiplied by 1.1 or not, the CBB test yields a TDR superior to 90 % for an enrichment level of 20 wt% ($TDR = 0.976$, Fig. 18).
2) For an integration time $t = 500$ s and a stationary background, the CNB test yields a TDR superior to 90 % for an enrichment level of 1 wt% ($TDR = 0.945$, Fig. 16)
3) From point 1 and 2, we can conclude that there is at least a hypothesis test able to achieve a compromise TDR/FAR exceeding the factor of merit 50 % / 90 % with a measurement time of 500 s, in the case of a stationary background
4) Whether the background is multiplied by 1.1 or not, for a measurement time $t = 3000$ s, the CBB test gives access to a TDR strictly superior to 90% for any enrichment level ($TDR = 0.932$, Fig. 16 ; $TDR = 0.902$, Fig. 17 ; $TDR = 0.999$, Fig. 18)

Point 3 supports the deployability of this solution as a “first level” detector, used to assess the measured surface before employing any other detectors, in a reasonable time. Considering a representative basic nuclear facility with a total surface to assess of a hundred thousand square meters, a measurement time of 5 minutes per square meter results in a total study time of 350 days.

Point 4 underlines the ability to deploy this solution as a “second level” high performance detector, used to confirm the suspicion of a contamination, detected with another instrument which response time is lower (contamination meters for example). Such a confirmation can be expected with a compromise TDR/FAR of 50 % / 100 % and a measurement time under one hour per square meter.

VIII. General conclusion and outlooks

We recall here that the objective of this paper was to study the feasibility of a gamma spectrometry method to decommission nuclear basic facilities, regarding low uranium contamination. The first result of this concept study is the establishment of a complete methodology, dedicated to the dimensioning and the characterization of a technological solution to the considered problem. This methodology is based on the construction of:

- A varying gamma-ray source term as a function of the uranium surface activity and the enrichment level of ^{235}U
- A model of an HPGe detector with MCNP6.1 and calibrated using standard sources
- ROC curves allowing connecting, under the hypothesis of a minimal surface activity to detect and an acceptable false alarm rate, a true detection rate and a radiological characterization time

As we said in the introduction, alpha signal, beta signal and gamma signal coming from uranium form three measurands that can be used alternatively or, as a way to consolidate the alarm, cumulatively. In the latter, the question is to know which measurand is exploited by a "first level" detector, which reliable response time must be the fastest possible, and which measurand has to be used with a "second level" detector, as a confirmation for an alarm.

For a minimal surface activity to detect of A = 2000 Bq (α) / m², Ω = 2π sr, the algorithms tools developed enable us to envision a TDR/FAR compromise exceeding the factor of merit 50 % / 90 % with a measurement time of 500 s / m², under the hypothesis that the background signal is stationary (else, exceeding a factor 50 % / 70 %). This observation support the deployability of the proposed solution as a "first level" detector, used to scan the assessed surface before any other instrument. This technological option is important in the case of the impossibility to use alpha and beta measurands. Finally, the usage of plural HPGe detection heads would enable to refine the localization of the contamination as well as reducing the measurement time per square meter.

In the case of high detection limits (which is true for low enrichment levels), of the dispersion of the distribution (both in shapes and amplitudes), and of the difficulties behind the handling of HPGe detectors (cooling, fragility, clutter), the most credible scenario is the usage of the presented method as a "second level" detector. Such a usage withdraw the time constraint but impose a drastic minimization of the beta risk (wrong non-detection or false alarm). Yet, we found that raising the measurement time to 3000 s / m² and considering a stationary background signal (which is a reasonable hypothesis, since a background signal measurement will be conducted *ad hoc*), the CNB test factor of merit exceeds 50 % / 99 % for any enrichment level. Table VII and VIII sum up the results mentioned in this conclusion. We calculated a radiological characterization time, which corresponds to the measurement time times the example BNF surface.

Table VII. *Characteristics and estimations of the factors of merit of the proposed solution for a "first level" detector, stationary background*

Basic nuclear facility surface	**Enrichment level (^{235}U)**	**Measurement time**	**FAR**	**TDR**	**Radiological characterization time**
100000 m²	1 wt%	500 s / m²	50 %	94.6 %	578 d (3.6 y)
100000 m²	3 wt%	500 s / m²	50 %	97.9 %	578 d (3.6 y)
100000 m²	8 wt%	500 s / m²	50 %	99.6 %	578 d (3.6 y)
100000 m²	20 wt%	500 s / m²	50 %	99.9 %	578 d (3.6 y)

Table VIII. *Characteristics and estimations of the factors of merit of the proposed solution for a "second level" detector, stationary background*

Basic nuclear facility surface	**Enrichment level (^{235}U)**	**Measurement time**	**FAR**	**TDR**
100000 m²	1 wt%	3000 s / m²	50 %	99.9 %
100000 m²	3 wt%	3000 s / m²	50 %	99.9 %
100000 m²	8 wt%	3000 s / m²	50 %	>99.9 %
100000 m²	20 wt%	3000 s / m²	50 %	>99.9 %

Obtained results in the framework of this study lead us to consider the following outlooks:

1) We have generated ROC curves and true detection rate as a function of the measurement time curves, based on the minimal surface activities to detect, using MCNP6.1. We also used data from

experimental measurements on contaminated and non-contaminated surfaces. Since we do not know precisely the enrichment level, it is impossible to link the results to the minimal surface activity to detect. We propose the development of concrete sample where a precise contamination of uranium is layered, enabling us to calibrate the ROC and the TDR/time of measurement curves. We will also study the matrix effect, consequence of the state of the concrete surfaces.

2) As we stated in II. A. and C., we have a physical model of the gamma source term, associated to a uranium surface contamination. This model will be used as an *a priori* in the construction of the H_1 hypothesis. For such an approach, we have developed Bayesian statistical tests, competing with CNB and CBB, with promising performances [36]. Future work will be devoted to the study of the usage of the Bayesian tests in this context: we propose to duplicate the characterization studies presented in VI using the Bayesian tests.

3) Using innovative HPGe detectors, such as ones with an anti-Compton shield, can be studied to reduce the impact of the background signal [16, 37]

Acknowledgements

The authors would like to thank the teams of P. Bourrelier from ORANO CYCLE, and of G. Aubert and J. Baticle from ORANO DS, for their help in writing this paper.

References

[1] E. Neri, *et al.*, *Costs of Decommissioning Nuclear Power Plants (NEA--7201)*, Nuclear Energy Agency of the OECD (NEA), 2016.

[2] S. Aggarwal, *Alpha-particle spectrometry for the determination of alpha emitting isotopes in nuclear, environmental and biological samples: Past, Present and Future*, Anal. Methods. 8. 10.1039/C6AY00920D, 2016.

[3] P. Fichet, A. Leskinen, S. Guegan, F. Goutelard, *Characterization of Beta Emitters for Decommissioning,* ASME, International Conference on Radioactive Waste Management and Environmental Remediation, Volume 2: Facility Decontamination and Decommissioning; Environmental Remediation; Environmental Management/Public Involvement/Crosscutting Issues/Global Partnering, Brussels, Belgium, September 8–12, 2013.

[4] J. C. J. Dean, *et al*., *Traceability for measurements of radioactivity in waste materials arising from nuclear site decommissioning*, Metrologia 44 S140–S145, 2007.

[5] G. R. Gilmore, *Practical Gamma-ray Spectrometry*, 2nd Edition, John Wiley & Sons Ltd, The Atrium, Southern Gate, Chichester, West Sussex, England, pp. 41-47, 2008.

[6] B . Pérot *et al.*, *The characterization of radioactive waste: a critical review of techniques implemented or under development at CEA, France*, EPJ Nuclear Sci. Technol. 4 3, 2018.

[7] AC02459866, ed. *Radiological characterization of shut down nuclear reactors for decommissioning purposes*, International Atomic Energy Agency, 1998.

[8] T. Z. Nonova, *et al.*, *Radiological characterization activities during the partial dismantling of the IRT-SOFIA research reactor facilities*, Romanian Journal of Physics, 59(9-10), pp. 976-998, 2014.

[9] A. Savidou, *et al.*, *Non-destructive technique to verify clearance of pipes*, Nuclear Tech. and Rad. Prot., Vol. 25 N°2, pp. 133-137, 2010.

[10] R. Venkataraman, *et al.*, *Validation of in situ object counting system (ISOCS) mathematical efficiency calibration software*, Nuclear Instruments and Methods in Physics Research Section A: Accelerators, Spectrometers, Detectors and Associated Equipment, Vol. 422, pp. 450-454, 1999.

[11] A. Alvarez, *et al*., *Uranium determination in samples from decommissioning of nuclear facilities related to the first stage of the nuclear fuel cycle*, Applied Radiation and Isotopes, Vol. 53 1-2, pp. 355-359, 2000.

[12] J. Boson, *Improving accuracy of in-situ gamma-ray spectrometry*, doctoral dissertation, Radiofysik, 2008.

[13] A. Stepanov, *et al.*, *Development and Application of Collimated Spectrometric Systems for the Characterization of Radioactive Contamination of Decommissioned Facilities – 15030*, Proceeding of the 15th Waste Management Conference, Phoenix, Arizona, USA, 2015.

[14] V. E. Stepanov, *et al.*, *Remote-controlled collimated gamma-ray detector for measuring radioactive contamination*, Atomic Energy, Vol. 109, N°2, pp.82-84, 2010.

[15] S. Garti, Q. Lecomte, J. Dumazert, K. Bourdergui, C. Jammes, *A high sensitivity Compton Suppressor System for nuclear waste characterization*, ISOE European Symposium, Uppsala, 26-28 June 2018

[16] S. Garti, J. Dumazert, R. Coulon, Q. Lecomte, F. Carrel, G. Corre, M. Imbault, *et al.*, *Characterizing low-activity waste containers: a case study for Compton Suppression Systems under challenging signal-to-noise ratio*, Nuclear Inst. and Methods in Physics Research, A, *in press*, 2019.

[17] M.-M. Bé, V. Chisté, *Table de radionucléides*, LNE-LNHB/CEA, 2007.

[18] Y. Y. Ebaid, *Use of gamma-ray spectrometry for uranium isotopic analysis in environmental samples*, Romanian Journal of Physics, Vol. 55, N° 1-2, pp. 69-74, 2010.

[19] M. Hult, E. Andreotti, R. González de Orduña, S. Pommé, Y. Yeltepe, *Quantification of uranium-238 in environmental samples using gamma-ray spectrometry*, EPJ Web of Conferences, Vol. 24, 07005, 2012.

[20] M. Tsutsumi, T. Oishi, N. Kinouchi, R. Sakamoto, M. Yoshida, *Simulation of the background for gamma detection system in the indoor environment of concrete buidings*, Journal of Nuclear Science and Technology, Vol. 38, N° 12, pp. 1109-1114, 2001.

[21] T. Marchais, B. Pérot, C. Carasco, P.-G. Allinei, P. Chaussonnet, J.-L. Ma, H. Toubon, *Gamma-ray spectroscopy measurements and simulations for uranium mining*, EPJ Web of Conferences, Vol. 170, 05003, 2018.

[22] A. Sari, F. Carrel, F. Lainé, *Characterization and Optimization of the Photoneutron Flux Emitted by a 6- or 9-MeV Electron Accelerator for Neutron Interrogation Measurements*, IEEE Transactions on Nuclear Science, vol. 65, no. 9, pp. 2539-2546, 2018.

[23] D. B. Pelowitz (Ed.), *MCNP6™ User's Manual Version 1.0*, Los Alamos National Laboratory report, LA-CP-13-00364, Rev. 0, 2013.

[24] A. L. Schwarz, R. A. Schwarz, and A. R. Schwarz, *MCNPX/6© Visual Editor Computer Code Manual*, 2018.

[25] *Evaluation of measurement data. Guide to the Expression of Uncertainty in Measurement*. Joint Committee for Guides in Metrology–JCGM 100, ISO/IEC Guide 98–3, http://www.iso.org/sites/JCGM/GUM-introduction.htm, 2008 (last visited 21/05/2019).

[26] K. R. Murphy, B. Myors, A. Wolach, *Statistical Power Analysis, A Simple and General Model for Traditional and Modern Hypothesis Tests, Fourth Edition*, 2014.

[27] A. A. Jarrett, *Statistical methods used in the measurement of radioactivity with some useful graphs and nomographs*, No. AECU-262, 1946.

[28] T. H. Wonnacott, R. J. Wonnacott, *Introductory statistics*, 5th Edition, chapter 19, 1990.

[29] D. K. Fagan, S. M. Robinson, R. C. Runkle, *Statistical methods applied to gamma-ray spectroscopy algorithms in nuclear security mission*, Applied Radiation and Isotopes, Vol. 70, Iss. 11, pp. 2428-2439, 2012.

[30] F. J. Massey, *The Kolmogorov-Smirnov Test for Goodness of Fit*, Journal of the American Statistical Association, 46:253, 68-78, DOI: 10.1080/01621459.1951.10500769, 1951.

[31] P. R. Rider, *The Negative Binomial Distribution and the Incomplete Beta Function*, The American Mathematical Monthly, vol. 69, no. 4, pp. 302–304, 1962.

[32] R. R. Wilcox, *A Review of the Beta-Binomial Model and its Extensions*, Journal of Educational Statistics, 6(1), 3–32, 1981

[33] J. Harold, *An invariant form for the prior probability in estimation problems,* Proceedings of the Royal Society A, 186, 1946

[34] C. E. Metz, *Basic principles of ROC analysis*, Seminars in Nuclear Medicine, Volume 8, Issue 4, Pages 283-298, ISSN 0001-2998, 1978.

[35] MATLAB 2017a, The MathWorks, Natick, 2017

[36] E. Barat, T. Dautremer, N. Dufour, J. Dumazert, *Procédé de détection des faibles activités radiologiques et produit-programme d'ordinateur associé*, French Atomic Energy Commission, Patent pending, 2019.

[37] R. Coulon, J. Dumazert, S. Garti, Q. Lecomte, *Système de spectrométrie, procédé de spectrométrie et produit programme d'ordinateur associés*, French Atomic Energy Commission, Patent deposited on 27/09/2018 under n° FR1858897, 2018.